High Energy Physics and Nuclear Physics

Volume 21, Number 2

Bi-dimension Position Sensitive Detector Used in the Study of Fusion Fission of Heavy Ions at the Sub-Coulomb Barrier Energy Region

Tan Jilian, Zhang Jinxia, Jin Genming, Zhang Huanqiao[1], Qian Xing[1], Liu Zuhua[1], and Xu Jincheng[1]

(Institute of Modern Physics, The Chinese Academy of Sciences, Lanzhou, China)
[1](China Institute of Atomic Energy, Beijing, China)

The structure, operation principle, and performance of the bi-dimension position sensitive avalanche chamber (BPAC) used in the study of fusion fission induced by heavy ions at the near- and sub-barrier energy regions are described.

The fold angle distribution of fragments in different angle regions for the 84 MeV (E_{cm}) $^{16}O+^{232}Th$ reaction system was obtained by using BPAC, from which the angle distribution of transfer-fission fragments has been distinguished from that of compound nucleus fission fragments. It is thereby certified that transfer fission is not the reason for anomalous anisotropies of fragment angular distribution. Meanwhile experimental results supported the pre-equilibrium fission model, in the frame of which the anomalous anisotropies of fragment distribution were explained.

Key words: fusion fission, position sensitive avalanche chamber, angle distribution of fragments.

Received December 12, 1995.

1. INTRODUCTION

The anomalous anisotropies of fission fragments were observed recently in heavy ion-induced fusion at near- and sub-barriers [1], and several interpretations for their origin were also presented. Almost all of interpretations were based on the inclusive measurements and with an assumption of fissioning nuclei being the compound of complete fusion. The angular distribution measured inclusively involves contributions from all possible reaction mechanisms, e.g., transfer fission, fusion fission, etc., and it is very difficult to separate out the contribution from a single process. In fact, a large part of the anomalous anisotropies in the reactions with targets of U, Th, and Np which are easily fissionable, is contributed by transfer fission. The difference between the folding angles of two fragments produced by different processes, which related to the corresponding linear momentum transfer or recoil velocity, could be used to distinguish the reaction mechanism of the fissioning nuclei. This will provide more reliable information for the interpretation of the anomalous fragments anisotropies peaking near 5 MeV below the Coulomb barrier.

The parallel plate avalanche counter (PPAC) which is characterized by its good timing, its capability of being easily made, its large active area, its working reliability, its capability to withstand a high count rate, and its insignificant irradiation damage is more and more widely applied as an important method of timing in nuclear experiments. To meet the need of angular distribution measurement, PPAC has been developed to be a one- or two-dimensional detector with a large active area. This detector is quite suitable for fold angle measurement and thus provides a good condition for experimental investigation of the anomalous anisotropies of fragments in heavy ion-induced fusion fission at the near- and sub-barriers.

2. STRUCTURE, ELECTRIC FIELD DISTRIBUTION

The sensitive area of the bi-dimension position sensitive avalanche chamber (BPAC) is 250 × 200 mm^2. The BPAC consists of four electrodes: anode A, grids K and G, and cathode C. The gaps between the electrodes are S_1, S_2, and S_3 (as shown in Fig. 1). The anode is a thin mylar foil (1.5 μm thick) uniformly evaporated with gold. The cathode was made of PCB. The K electrode is a wire grid with 20-μm gold-plated tungsten wires placed parallel to each other. The wire spacing is 1 mm. The wires are grouped in 4-mm-wide bins and soldered together to a tapped (LC) delay-line for the position determination in the x-coordinate. The structure of the G electrode is the same as the K-grid for the

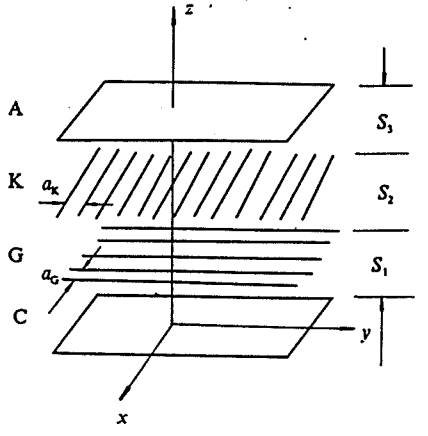

Fig. 1
The schematic structure of BPAC.

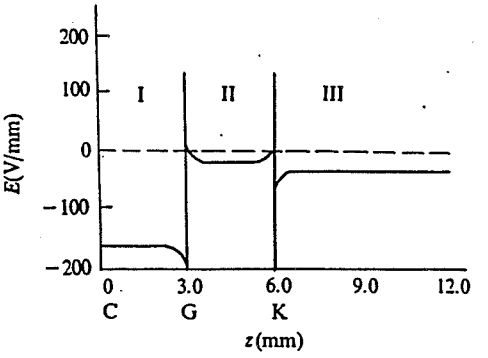

Fig. 2
The electric field in the BPAC.

position determination in the y-coordinate except that the wire spacing is 0.5 mm. If different voltages are applied to the electrodes, the field distribution in the sensitive volume of the detector is complicated. To simplify discussion and not lose generality, the potentials on electrodes, $V_A > V_K > V_G > V_C$ were supposed. The BPAC can be considered to consist of 3 capacitors. Thus the electric field strength at any point in the sensitive volume of the detector can be deduced from the surface charge density and the capacitance value [2] of the unit area of the capacitors:

$$E_x = \frac{2\pi\sigma_G \sin(2\pi x / a_K)}{\sin^2(\pi x / a_G) + \sinh^2(\pi(z - S_1) / a_G)}, \tag{1}$$

$$E_y = \frac{2\pi\sigma_K \sin(2\pi y / a_K)}{\sin^2(\pi y / a_K) + \sinh^2(\pi(z - S_1 - S_2) / a_K)}, \tag{2}$$

$$E_z = -2\pi\sigma_A + 2\pi\sigma_C + \frac{\pi\sigma_G \sinh(2\pi(z - S_1) / a_G)}{\sin^2(\pi x / a_G) + \sinh^2(\pi(z - S_1) / a_G)} + \frac{\pi\sigma_K \sinh(2\pi(z - S_1 - S_2) / a_K)}{\sin^2(\pi y / a_K) + \sinh^2(\pi(z - S_1 - S_2) / a_K)}, \tag{3}$$

where σ_A, σ_K, σ_G, and σ_C, are the surface charge densities of A, K, G, and C electrodes, respectively, and a_K, a_G are the wire spacings of K and G electrodes, respectively. The values of S_1, S_2, and S_3 are 3, 3, and 6 mm, respectively, for the BPAC described here. The voltages of +310 V, +70 V, 0 V, and −510 V were applied to the A, K, G, and C electrodes, respectively. A plot of calculated field strength in BPAC was shown in Fig. 2. By looking at Fig. 2 we can see that the field is uniform in a large region far from wires (beyond $\phi 100$ μm), and one may distinguish three regions with quite different field values, denoted by I, II, and III, respectively, where I and III are avalanche regions, II is the drift region; in the vicinity of the wires, the electric field is very strong and sharp.

If one does not consider the difference between plate and grid plane, the electric field strength in any region (e.g., G-C region) of BPAC is

$$E_{0GC} = (V_G - V_C) / S_1, \tag{4}$$

according to the result calculated above, the actual electric field is

$$E_{GC} = k(V_G - V_C) / S_1 = k E_{0GC}, \tag{5}$$

where

$$k = 1 / [1 + a_G / 2\pi S_1 \ln(a_G / 2\pi\rho_G)], \tag{6}$$

and ρ_G is the diameter of wires of the G electrode. It is seen in Eq.(6) that $E_{GC} < E_{0GC}$, and the ratio is k referred to as a field shield factor. The value of k increases with a decrease of wire spacing and with increase of wire diameter and gap between electrodes. Calculations indicate that if the spacing of wires increases from 0.5 mm to 3 mm, then the k value decreases from 0.948 to 0.619 when other conditions do not change. Therefore we could describe the electric field in the gap between a plate and a wire plane using the field in a region formed by two plates only in the case that spacing of wires is very small.

The field shield k' in the region formed by two wire planes (e.g., the gap between K and G) can be deduced by the same method:

$$k' = 1 / [1 + a_G / 2\pi S_2 \ln(a_G / 2\pi\rho_G) + a_K / 2\pi S_2 \ln(a_K / 2\pi\rho_K)], \tag{7}$$

where ρ_K is the wire diameter of the K electrode. From Eqs.(6) and (7) we see that the value of k' is smaller than that of k under same conditions.

3. OPERATION PRINCIPLE OF THE DETECTOR AND THE PERFORMANCE

3.1. Operation principle

When a charged particle passes through A electrode and enters the sensitive volume of the detector, it would lose partial energy and create electron-ion pairs along its path. A gas amplification process occurs when the electrons drift towards an anode in a strong field. In the vicinity of wires in the *k*-plane, due to the very high field, most probably a second amplification occurs. The signals are induced on the electrodes when the electron cloud drifts towards the anode. The signals extracted from the grid A and K via the L C delay line can determine the x, y two-dimensional coordinates. The signals extracted from C and A electrodes can measure the time and energy loss of incident particles, respectively.

3.2. Operating gas and the stabilization of the gas pressure

The detector is located in a vacuum chamber wherein the vacuum is better than 10^{-1}Pa, and connected into the gas source via a pipe. The detector is working with a gas-flowing mode. An automatic stabilization system which consists of an absolute gas pressure meter with a piezo-resistive pressure transducer, a control unit for a valve and an electromagnetic valve, is coupled with the vacuum pump. When the gas pressure in the detector is changed, the current signal from the control system will be fed back to the electromagnetic valve. The valve then adjusts the gas flow going into the detector to stabilize the pressure of gas. For a system satisfying a certain relation between the volume and the pump speed, the variation of gas pressure can be controlled within 1%.

We have used iso-butane, isobutylene, and n-heptane as working gas to test the performance of the detector and obtained fair results.

3.3. Selection of operating voltage and position resolution

There are three modes which can be selected for operating voltage supply.

(1) "Positive" supply: the potentials on electrodes C through A are supplied step up (C: −470 V, G: 0 V, K: +80 V, A: +350 V). The electrons produced by an avalanche effect will drift toward the A electrode. As stated above, a fast positive pulse with a rise-time of 3 — 4 ns will be produced on the C electrode; it can be used as a timing signal. The slower negative pulse with a rise-time of 15 ns from the A electrode is delayed about 40 ns more than the pulse of electrode C, and taken as a energy-loss signal of the incident particle. The pulses from electrodes G and K are all double-polarity signals with which both x and y positions can be read out through delay lines.

(2) "Negative" supply: the potentials from electrodes A to C step up (A: −600 V, K: −40 V, G: 0 V, C: +180 V). In this case the direction of the electric field and the drifting of an electron-ion pair, the polarities of pulses, and the time order that come from the electrodes are all opposite to that of the first case. Typical position spectra were shown in Fig. 3. In these two cases the variation of voltage of the K electrode will strongly affect the amplitude of output signals.

(3) The voltages supplied to the electrodes are as follows: A: −320 V, K: +320 V, G: 0 V, C: 460 V. The BPAC is actually subdivided into two independent detectors, C-G and G-K-A. In G-K-A, the electrons in the regions of G-K and K-A will all drift toward the K electrode. The negative signals are drawn from K-electrode. Due to the gas-gap difference between regions of G-K and K-A, the rise-times of signals coming from these two regions have a difference of several ns; however, the position can still be measured. Electrodes A and G produce positive pulses; the negative pulses are extracted from electrode C.

The selection of the operation mode should be determined by the test run for the physics experiments.

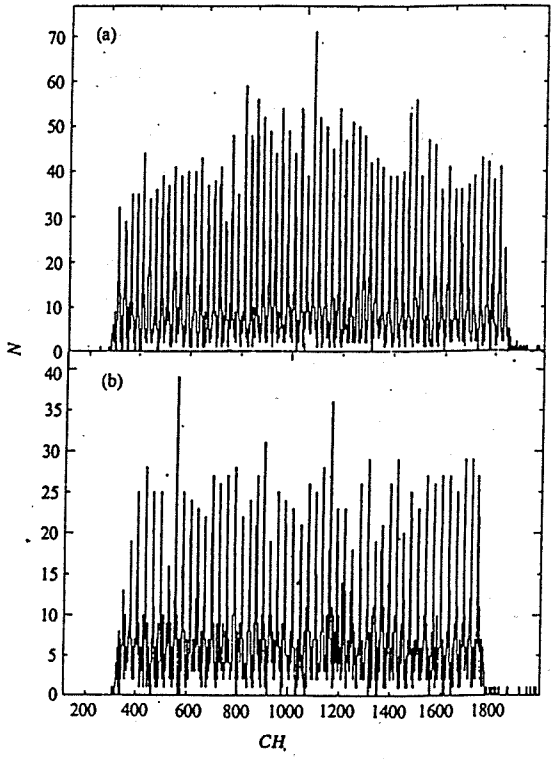

Fig. 3
Measured position spectra by using BPAC.
(a) x-position; (b) y-position.

3.4. Time resolution

The measurements of time resolution for BPAC are accomplished by using the time of flight method.

A PPAC is placed 60 mm in front of BPAC. Let the fragments from the fission source ^{252}Cf pass through two detectors. The start and stop time signals are obtained by using PPAC and BPAC, respectively. According to the flight-time spectrum, the time resolution of the BPAC is 680 ps (FWHM) (for light fragments). Considering the contributions from electronics and from the detector providing the start signals, the affections from the stretch of the mass and energy of ^{252}Cf, the delay fluctuation in BPAC, the intrinsic time resolution of BPAC is 290 ps.

3.5. Energy resolution

Adopting the first mode of voltage supply, the energy loss resolution $\delta(\Delta E)/\Delta E$ of BPAC is approximately 30%.

4. BPAC USED FOR THE EXPERIMENTAL STUDY OF NEAR- AND SUB-BARRIER FUSION FISSION

BPAC has been widely used in the research of heavy ion reaction mechanisms at intermediate energy, e.g., in the research of fusion fission at near- and sub-barriers. Zhang Huanqiao *et al.* from CIAE observed anomalous anisotropies of fragments in heavy ion-induced fusion fission at the energy

of 5 MeV below the barrier by using a mica trace detector. It is very important to perform measurements of the fragments from pure compound nuclei in the investigation of the anomalous anisotropies of fragments. Thus the BPACs described in this paper could be used to measure the fold angle of fragments and the timing signal, and to obtain the mass distribution of the fragments via kinematics reconstruction. The experiment was performed at HI-13 tandem accelerator in CIAE. Two BPAC were placed in the region from 10° to 90° and from 75° to 155°, respectively. The coincidence timing signal from the two BPACs was used as the trigger of each binary fission event. The result indicates that fusion-fission fragments and transfer-fission fragments can be distinguished clearly at their folding-angle distribution (see Fig. 4). It can be seen that there are two components in the folding-angle distribution: the one in the smaller folding angles is related to the transfer fission and the other one in larger folding angles is responsible to fusion fission. The difference between the average values of folding angles for the two components increases with increasing detection angles and this is consistent with the Monte Carlo simulation. So far the BPAC has been used to measure the fragment angular distributions and angular correlation for the system of $^{16}O+^{238}U$, $^{11}B+^{238}U$, $^{12}C+^{237}Np$, $^{16}O+^{237}Np$, and $^{19}F+^{232}Th$ at the near- and sub-Coulomb barriers. All of the results indicate that the

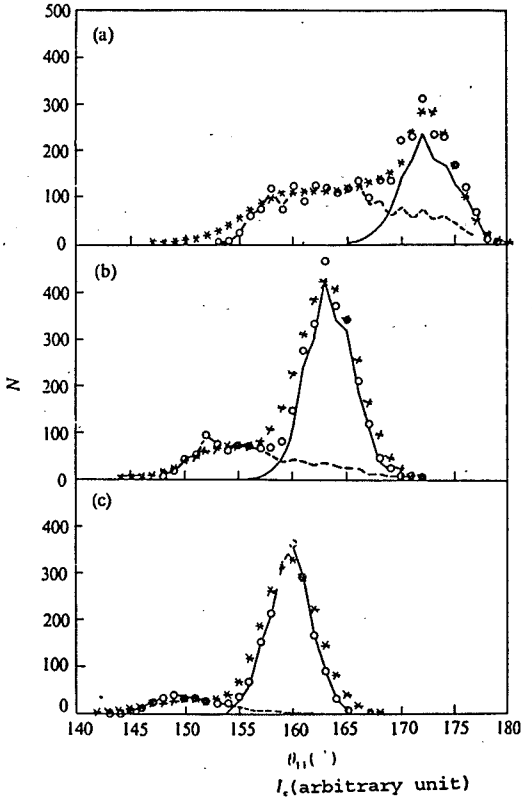

Fig. 4

The fold angle distribution at different fragment angle region of 84 MeV $^{16}O+^{232}Th$ reaction system.

* and o represent experimental data and the Monte Carlo simulation, respectively. The dashed line and solid line correspond to the simulated fold angle distribution of transfer fission and compound fission, respectively; (a), (b), and (c) denote angle regions of 10°—20°, 40°—50°, and 70°—80°, respectively.

anomalous anisotropies of fission fragments are still obvious after subtracting the transfer-fission component. Thus, it can be concluded that the transfer-fission is not the unique source for the measured anomalous anisotropies of fission fragments.

The results also indicate that the anomalous anisotropies of fission fragments at near- and sub-barriers are related to the mass asymmetry, α, of the incident system (see Fig. 2 in Ref. [4]). For the system with $\alpha > \alpha_{BG}$ (critical value), e.g., $^{11}B+^{238}U$, $^{11}B+^{237}Np$, $^{12}C+^{237}Np$, the experimental results are consistent with the calculation of the saddle point model, and this demonstrates that fusion-fission process goes through the spherical compound stage; thus it can be described by the saddle point transient state theory. The anomalous anisotropies of fission fragments for the systems with $\alpha < \alpha_{BG}$, e.g., $^{16}O+^{232}Th$, $^{19}F+^{232}Th$, and $^{16}O+^{238}U$, are obviously larger than that predicted by the saddle point model; this illustrates the fission process does not experience the thermalized compound stage and it still memorizes the incident system. The pre-equilibrium fission proposed in Ref. [4] can explain the anomalous anisotropies of fission fragments at the near- and sub-Coulomb barriers quite well.

In conclusion, BPAC has been successfully used in the experimental investigations of the heavy ion-induced fusion-fission at near- and sub-Coulomb barriers, and provided some reliable information for the explanation of the anomalous anisotropies of fission fragments at near- and sub-Coulomb barriers.

REFERENCES

[1] Zhang Huanqiao, *High Energy Phys. and Nucl. Phys.* (Chinese Edition), **16**(1992), p. 826.
[2] M. Mose *et al.*, *Methods of Theoretical Physics*, **2**(1953), p. 1234.
[3] Qian Xing, *High Energy Phys. and Nucl. Phys.* (Chinese Edition), **18**(1994), p. 385.
[4] Liu Zuhua *et al.*, *High Energy Phys. and Nucl. Phys.* (Chinese Edition), **20**(1996), p. 107.